Supporting Information

Polymer-inspired Covalent Triazine Frameworks from the Carbonaceous Side - Influence of Unexpected Surface Functionalisation on Liquid-Phase Adsorption Processes

Andree Iemhoff, ‡[a]Jeff Deischter, ‡[a] Shannon Jung, [a] Giulia Tuci, [b] Giuliano Giambastiani, [b,c,d] and Regina Palkovits, *[a]

[a] Chair of Heterogeneous Catalysis and Chemical Technology, ITMC, RWTH Aachen University, Worringerweg 2, 52074 Aachen, Germany. E-mail: palkovits@itmc.rwth-aachen.de

[b] Institute of Chemistry of OrganoMetallic Compounds, ICCOM-CNR and Consorzio INSTM, Via Madonna del Piano 10-50019, Sesto F.no, Florence, Italy

[c] Institut de Chimie et Procédés pour l'Energie, l'Environnement et la Santé (ICPEES), UMR 7515 CNRS-University of Strasbourg (UdS), 25, rue Becquerel, 67087 Strasbourg Cedex 02, France.

[d]Kazan Federal University, 420008 Kazan, Russian Federation

‡These authors contributed equally to this work.

Corresponding author: Regina Palkovits, palkovits@itmc.rwth-aachen.de

Table of Contents

Table S1. Detailed masses for the synthesis of CTF materials based on the $ZnCl_2$-route.

Monomer	Synthesis Temperature [°C]	m(monomer) [mg]	n(monomer) [mmol]	m($ZnCl_2$) [mg]	Monomer : $ZnCl_2$ (molar)
pDCB	400	600	4.68	3312	1:5
pDCB	400/600	600	4.68	3312	1:5
DCP	400/600	600	4.65	3169	1:5
DCBP	400/600	400	1.96	1335	1:5
DCP/DCBP	400/600	194 / 306	1.5 / 1.5	2043	1:5

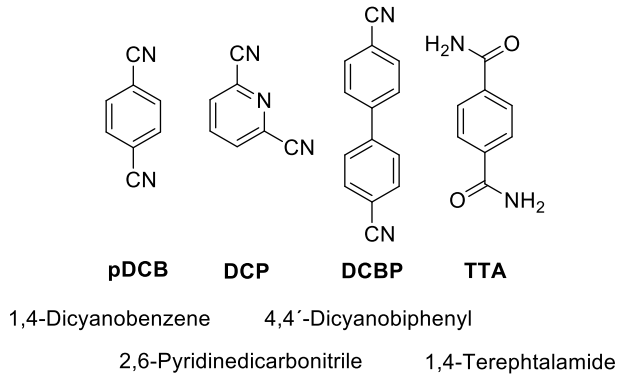

Figure S1. Overview of the monomers used in this study.

Table S2. Detailed masses for the synthesis of CTF materials based on the P_4O_{10}-route.

Monomer	Synthesis Temperature [°C]	m(monomer) [g]	m(monomer) [mmol]	m(P_4O_{10}) [g]	Monomer : P_4O_{10} (molar)
TTA	400	2.0	12.19	10	1:2.9
TTA	400/600	1.35	8.23	6.67	1:2.9

Table S3. Idealized values for elemental analysis of the CTF materials based on the monomers used for the respective synthesis.

Monomer	C / wt.%	H / wt.%	N /wt.%	O /wt.%
pDCB	74.9	3.1	21.9	N/A
DCP	65.6	2.3	32.5	N/A
DCBP	82.3	3.9	13.8	N/A
TTA	58.5	4.9	17.1	19.5

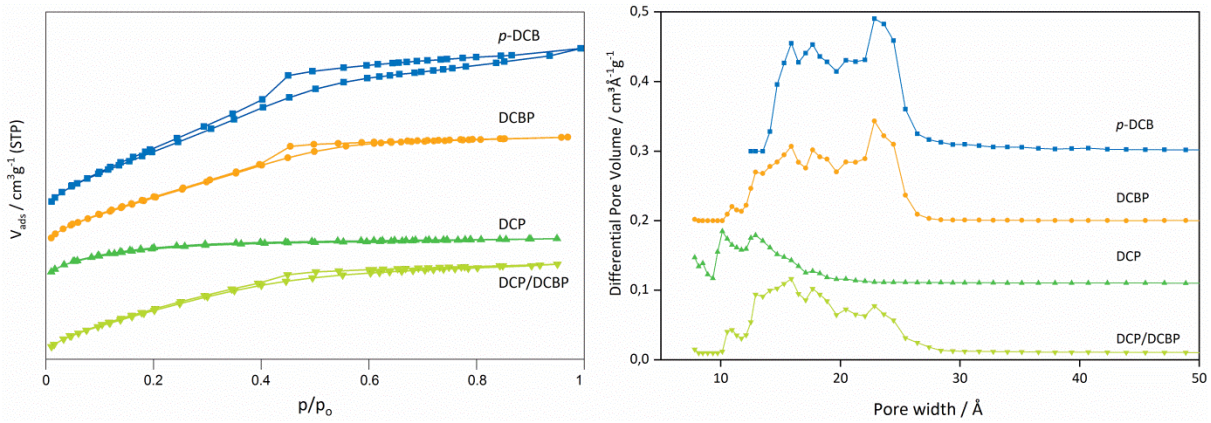

Figure S2. (left) Nitrogen physisorption adsorption-desorption isotherms of $ZnCl_2$ based CTF materials (offset: 200 cm^3g^{-1}), (right) DFT pore size distributions (offset: 0.1 $cm^3A^{-1}g^{-1}$).

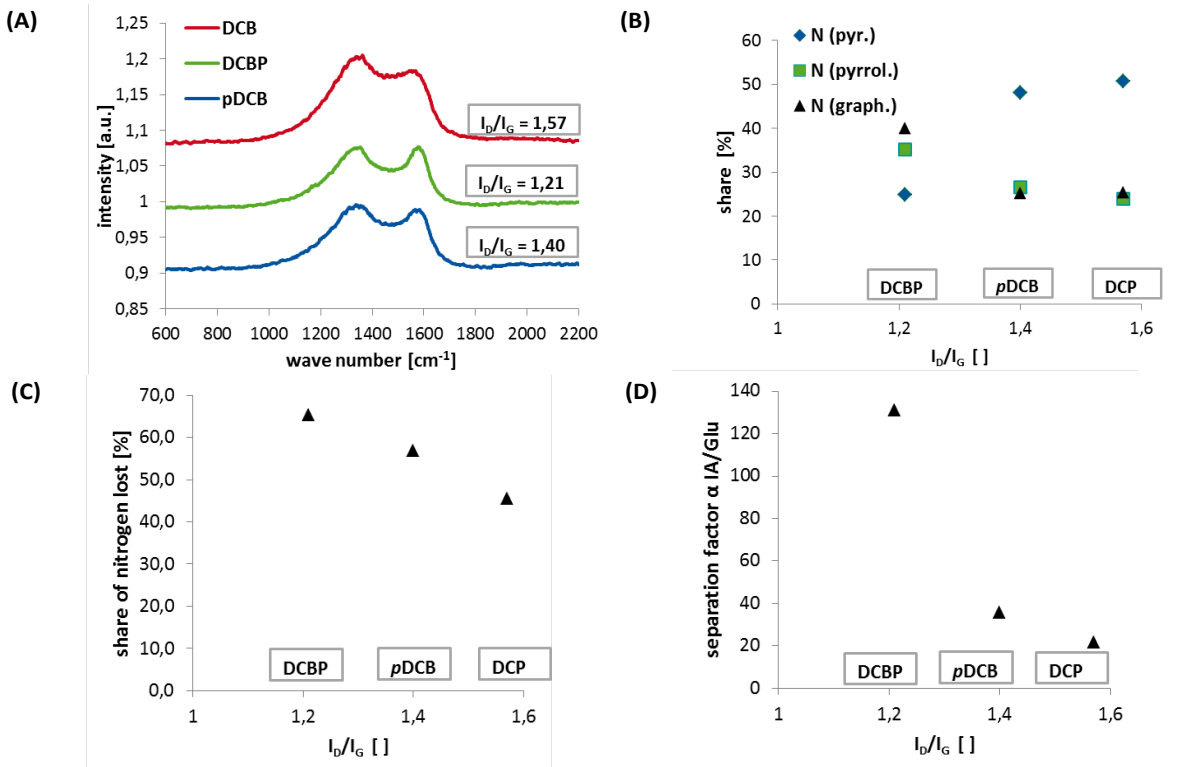

Figure S3. (A) Raman analysis of $ZnCl_2$-based materials synthesized from different monomers with respective I_D/I_G ratios after fitting. (B) Correlation of defectiveness of graphitized CTFs with the share of different nitrogen species as obtained from XPS analysis. (C) Correlation of defectiveness of graphitized CTFs with the degree of carbonization as expressed by the share of nitrogen lost during synthesis of CTFs based on different monomers. (D) Correlation of defectiveness of graphitized CTFs with the separation factor of IA/Glu.

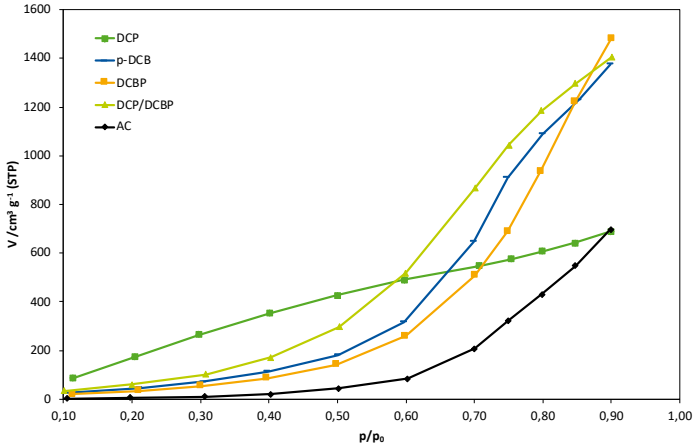

Figure S4. Water vapor adsorption isotherms of $ZnCl_2$ based materials at 25 °C. (AC = activated carbon, A Supra EUR, reference material)

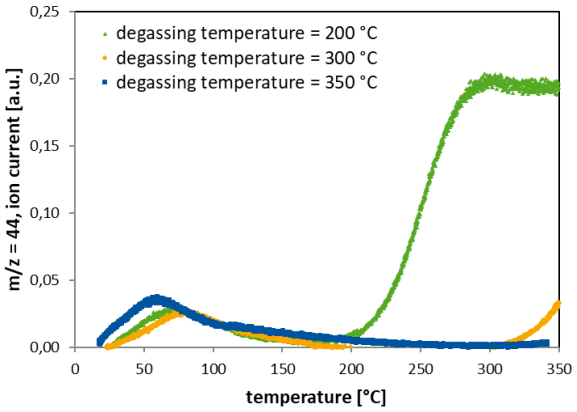

Figure S5. CO_2 desorption in dependence of the degassing temperature before CO_2 adsorption indicating the presence of surface functional group as opposed to freshly adsorbed CO_2 for desorption > 150 °C.
For the other materials (Table 1 entries 1,3 and 4) their lower density prevented the recording of desorption profiles due to sensitivity reasons.

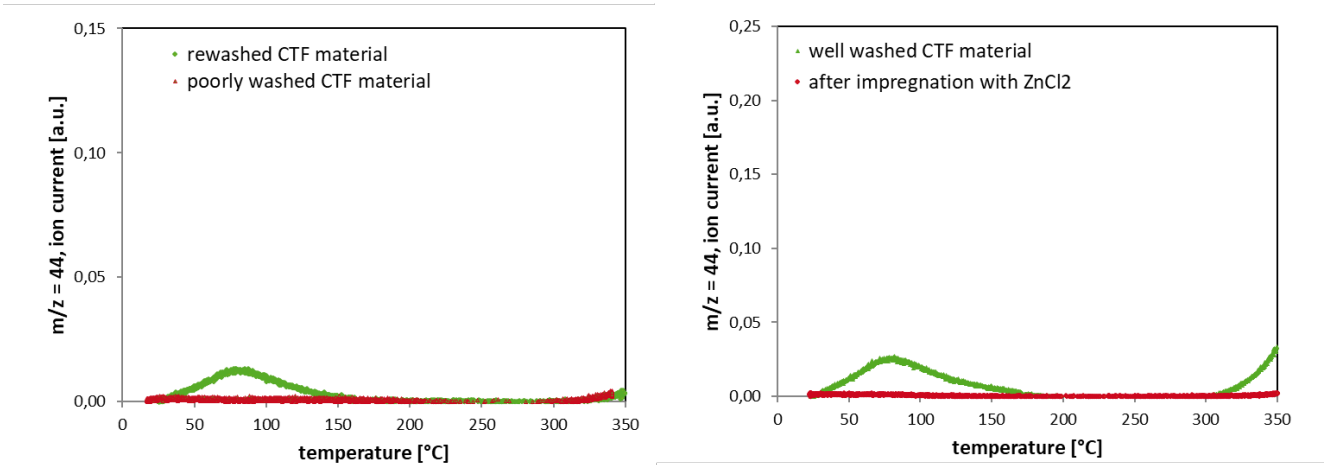

Figure S6. (left) Influence of repeated washing of a poorly-washed material on CO_2 desorption. (right) Influence of impregnation of a well-washed material with $ZnCl_2$ on CO_2 desorption.

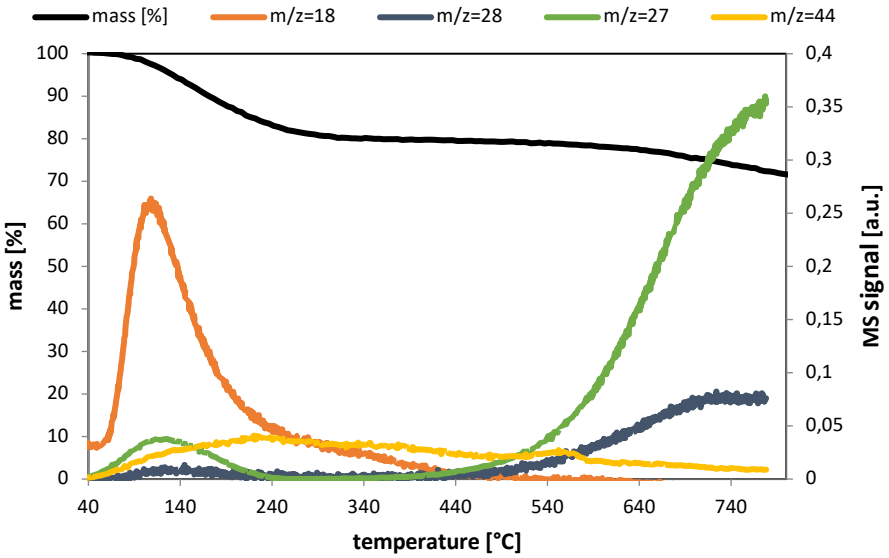

Figure S7. Representative TGA-MS of CTF-DCP showing temperature stability up to 480 °C. Also, the gap in mass balance compared to the monomers observed in elemental analysis (Table S1) can be explained by adsorbed water molecules, which desorb at around 200 °C.

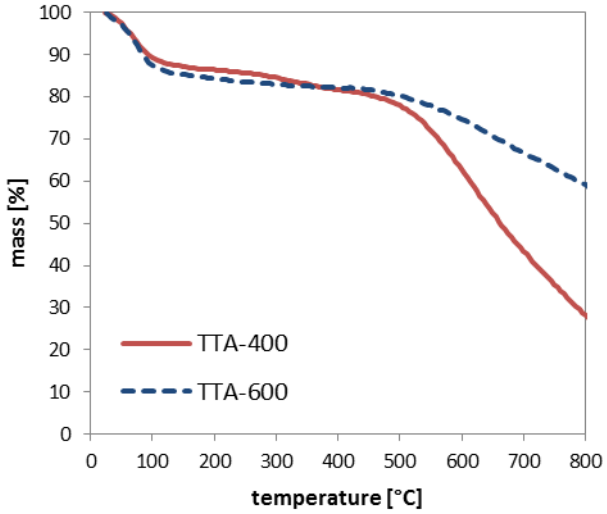

Figure S8. Thermogravimetric analysis of TTA-400 TTA-600 in nitrogen.

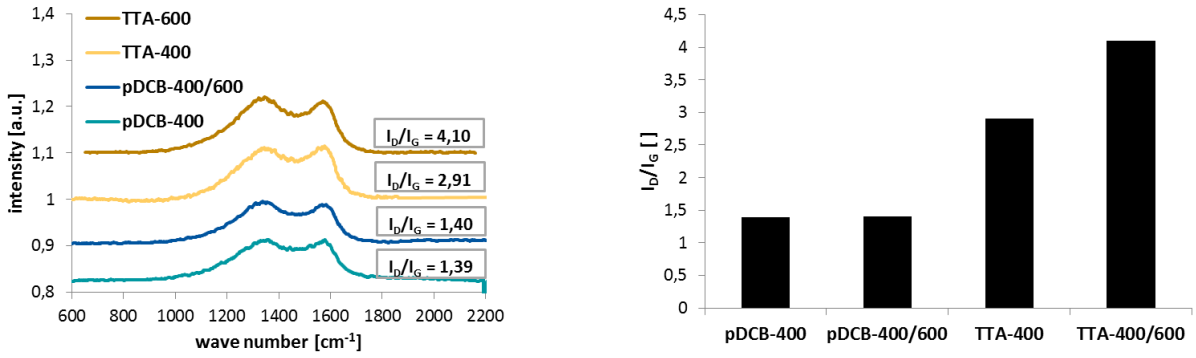

Figure S9. (left)Raman analysis of P_4O_{10}-based materials in comparison with $ZnCl_2$-based materials synthesized at different temperatures. (right) I_D/I_G values obtained from fitting Raman spectroscopic data showing a strong difference between $ZnCl_2$ and P_4O_{10}-based materials.

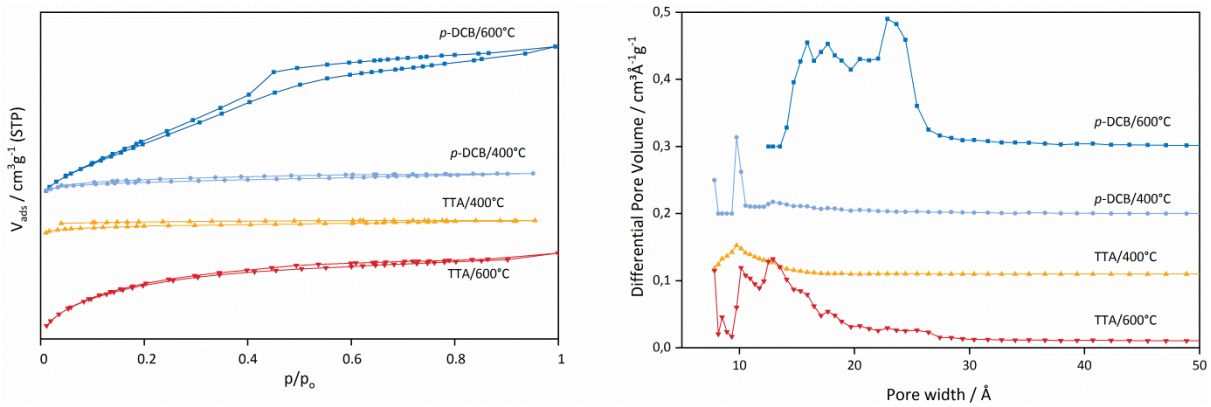

Figure S10. (left) Nitrogen physisorption adsorption-desorption isotherms of phosphorpentoxide based CTF materials (offset: 200 cm^3g^{-1}), (right) DFT pore size distributions (offset: 0.1 $cm^3A^{-1}g^{-1}$).

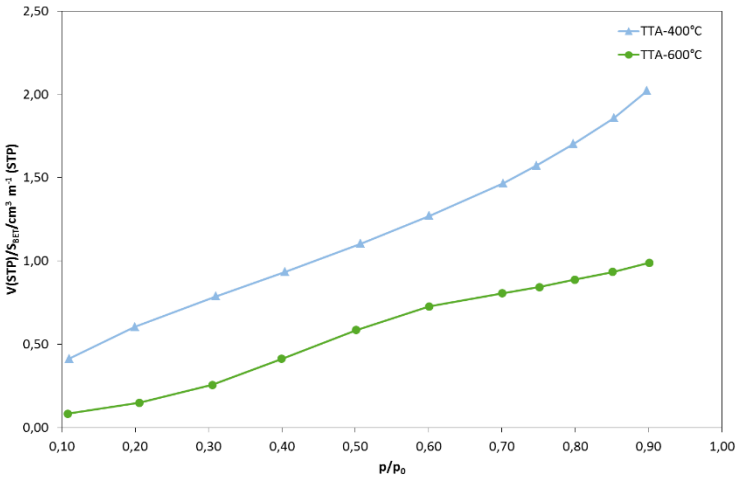

Figure S11. Water vapor adsorption isotherms of CTF materials based on the P_4O_{10}-route at 25 °C (normalized by specific surface area).

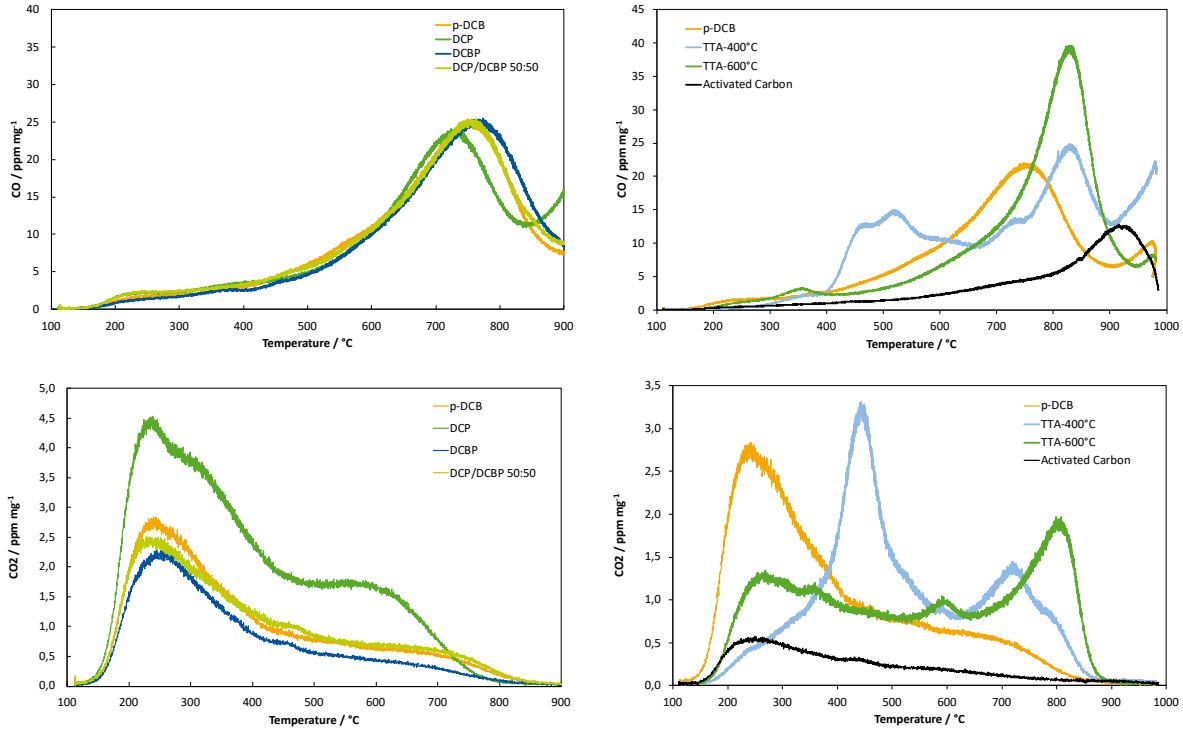

Figure S12. Rates of CO and CO_2 released during TPD-MS analysis of (left) CTF materials based on the $ZnCl_2$-route, (right) CTF materials based on the P_4O_{10}-route and activated carbon.

This process uses the relative thermal stability of surface functionalities to determine these on the carbon surface.[1, 2]

Table S4. Overview of elemental composition of CTF samples based on TTA at different temperatures derived from elemental and XPS analysis.

	Elemental analysis		
Sample	C [wt.%]	H [wt.%]	N [wt.%]
TTA-400°C	62.34	3.64	16.62
*p*DCB-400	73.64	3.11	16.75
TTA-600°C	73.51	1.74	10.4
*p*DCB-600	75.28	2.41	9.42

	XPS analysis							
Sample	C [at.%]	N [at.%]	O [at.%]	P [at.%]	C [wt.%]	N [wt.%]	O [wt.%]	P [wt.%]
TTA-400°C	72.5	9.6	16.6	1.4	66.3	10.2	20.2	3.3
*p*DCB-400	N/A				N/A			
TTA-600°C	78.4	6.8	13.4	1.4	72.7	7.4	16.5	3.4
*p*DCB-600	75.7	3.8	20.5	N/A	70.4	4.1	25.5	N/A

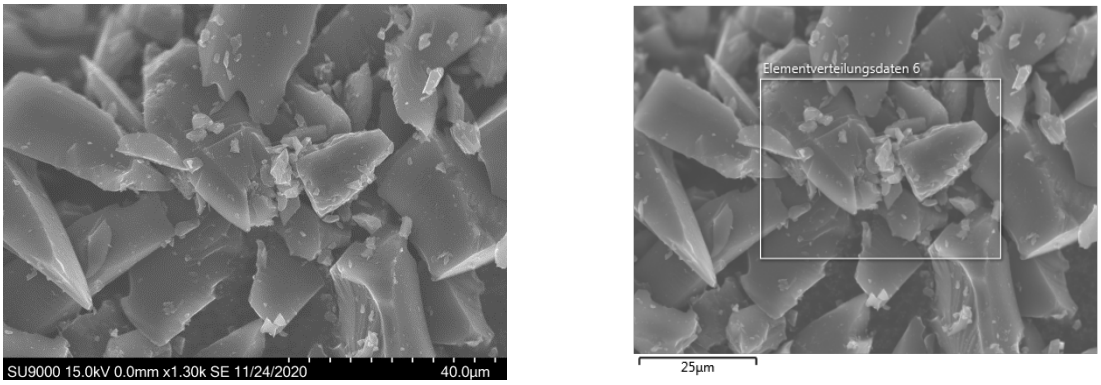

Figure S13 SEM-EDX microscopic measurement of *p*DCB-400/600. Overview (40 µm, right) and frame for EDX elemental mapping (right).

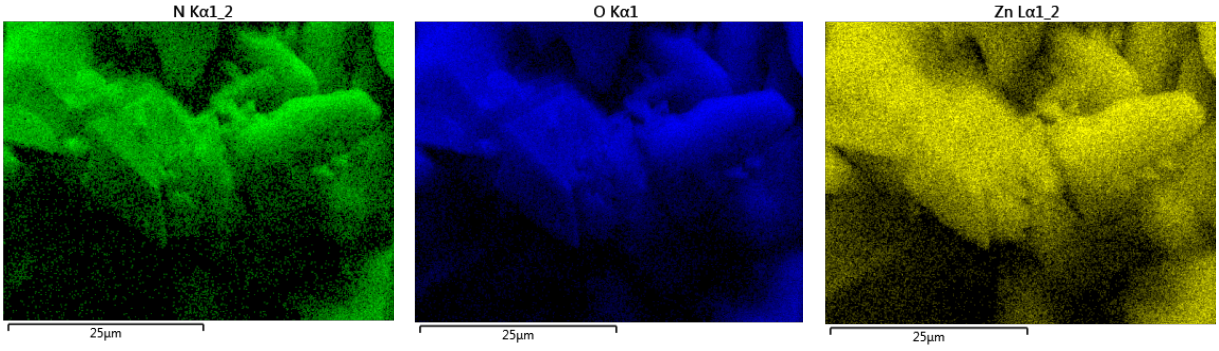

Figure S14. EDX elemental mapping of heteroatoms in *p*DCB-400/600 (N,O, Zn) illustrating a uniform distribution.

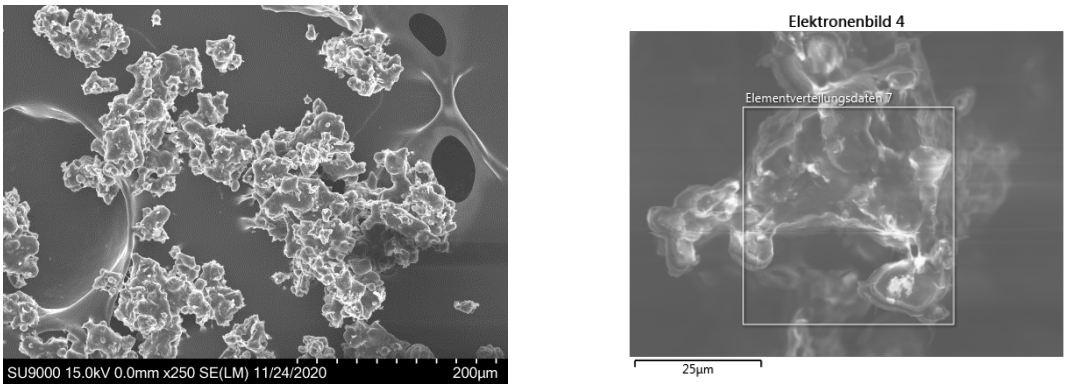

Figure S15. SEM-EDX microscopic measurement of TTA-400. Overview (200 µm, right) and magnification for EDX elemental mapping (right).

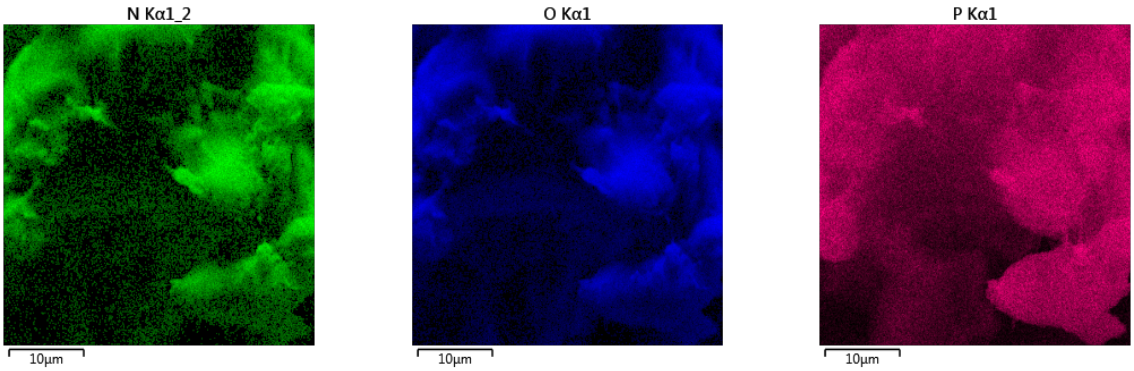

Figure S16. EDX elemental mapping of heteroatoms of interest in TTA-400 (N,O, P) illustrating a uniform distribution.

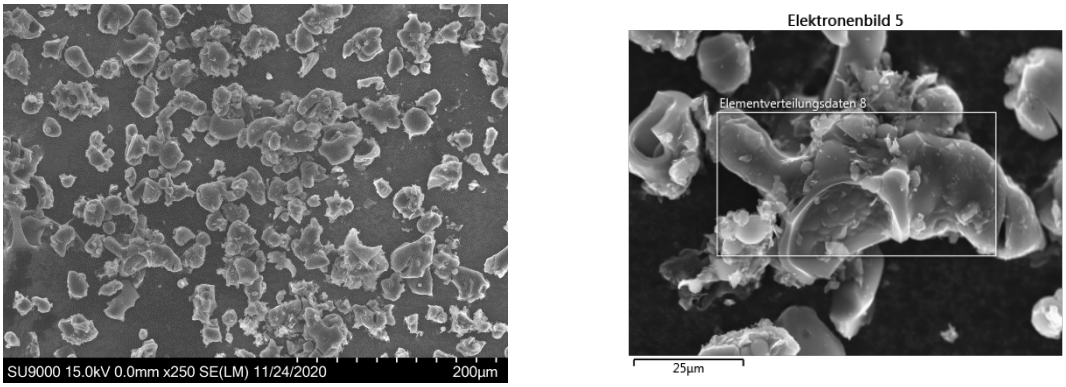

Figure S17. SEM-EDX microscopic measurement of TTA-600. Overview (200 µm, right) and magnification for EDX elemental mapping (right).

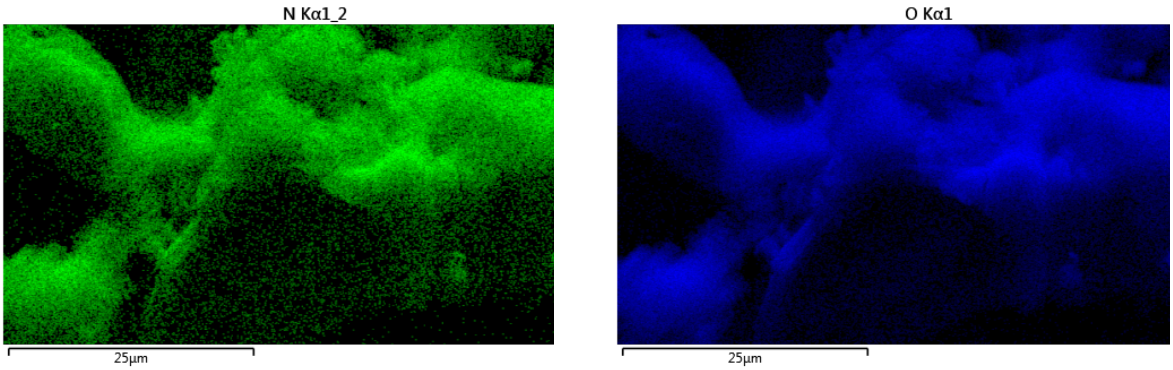

Figure S18. EDX elemental mapping of heteroatoms of interest in TTA-400 (N,O) illustrating a uniform distribution.

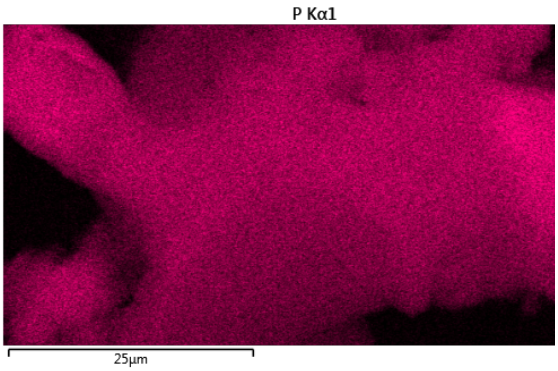

Figure S19. EDX elemental mapping of phosphorous in TTA-600 illustrating a uniform distribution.

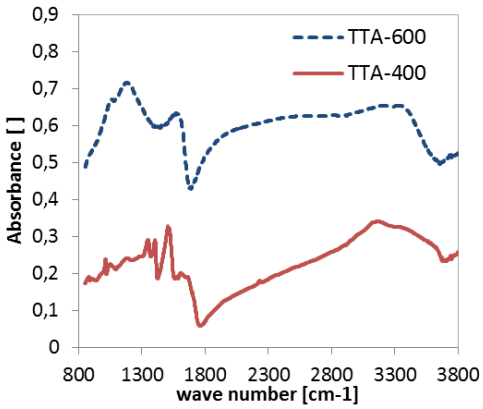

Figure S20. IR spectra of TTA-400 and TTA-600 illustrating the transition from a defined framework to a carbonized structure.

The spectra were recorded by Transmission IR spectroscopy. The black materials were ground together with KBr (0,5 wt.% sample in KBr), pressed to a pellet and dried in He(5.0) flow for 1 hour before measurement.

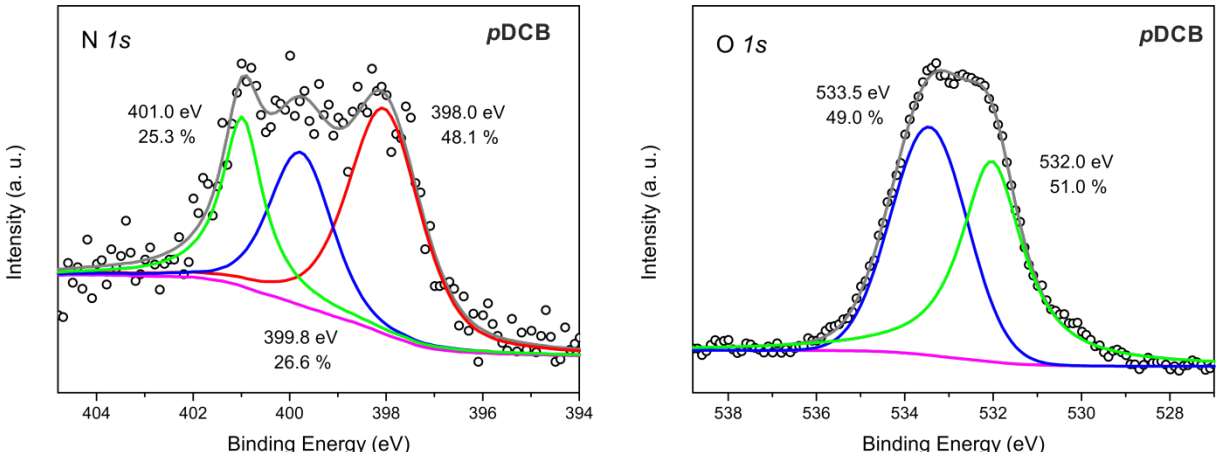

Figure S21. High resolution N1s and O1s core level region of pDCB sample along with their relative fitting.

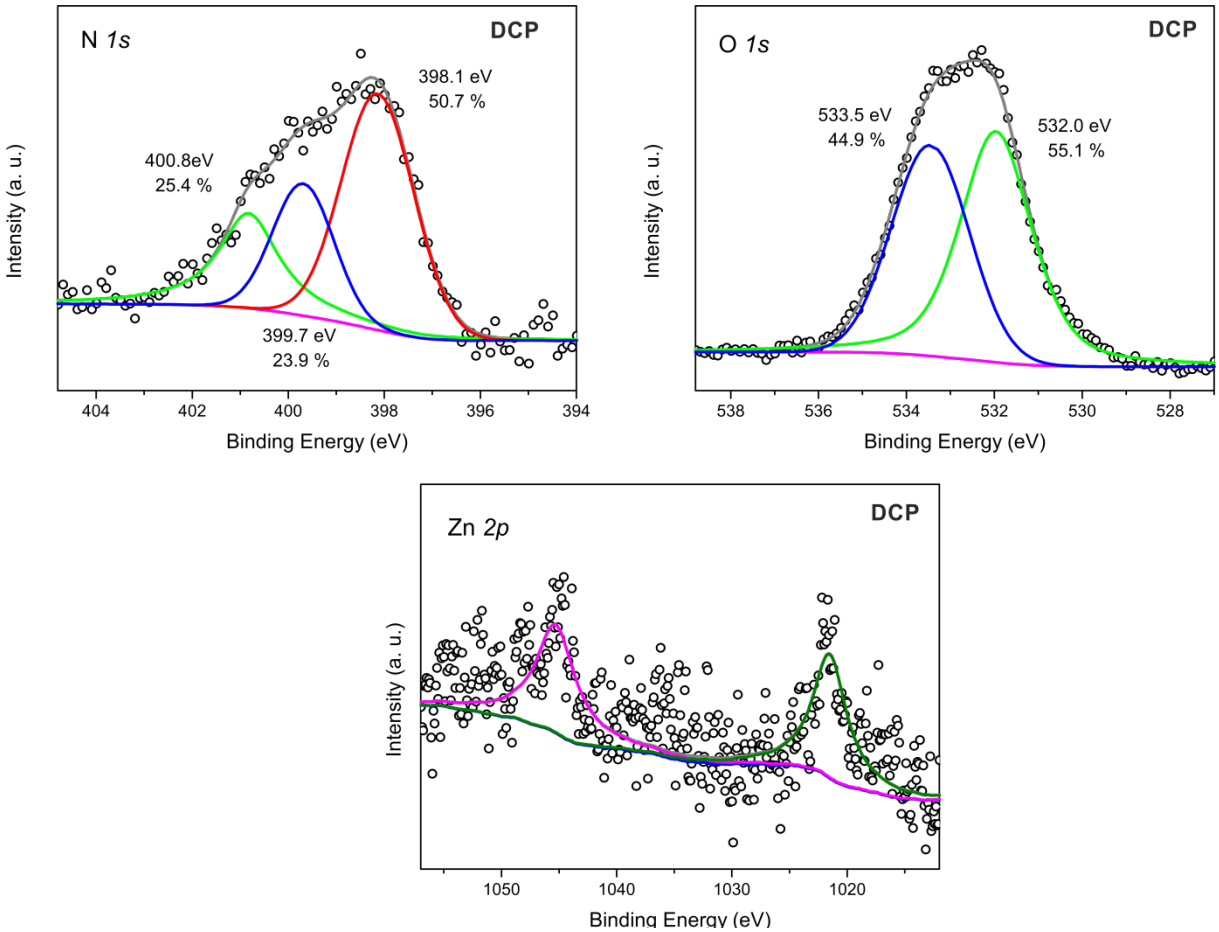

Figure S22. High resolution N1s, O1s and Zn2p core level region of DCP sample along with their relative fitting.

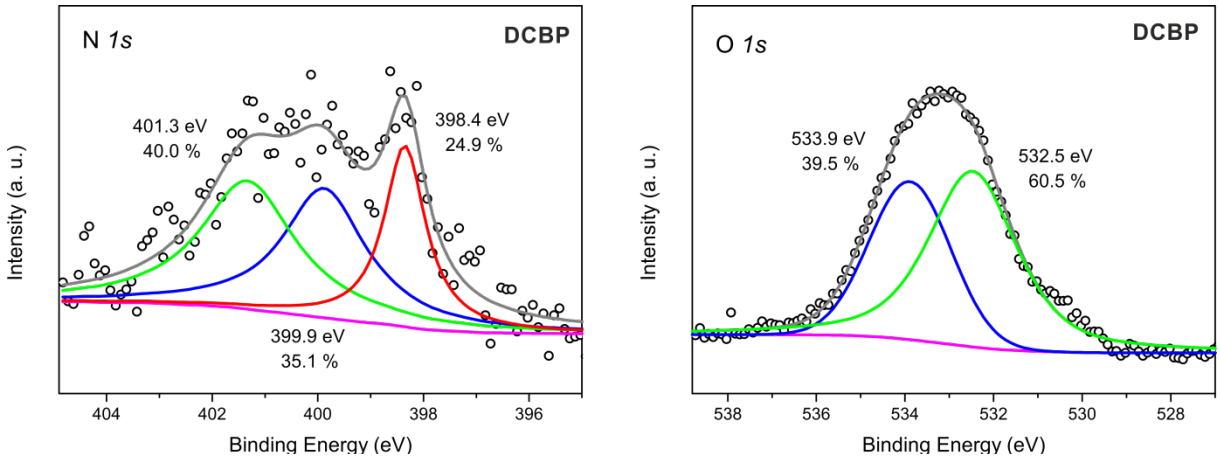

Figure S23. High resolution N1s and O1s core level region of DCBP sample along with their relative fitting.

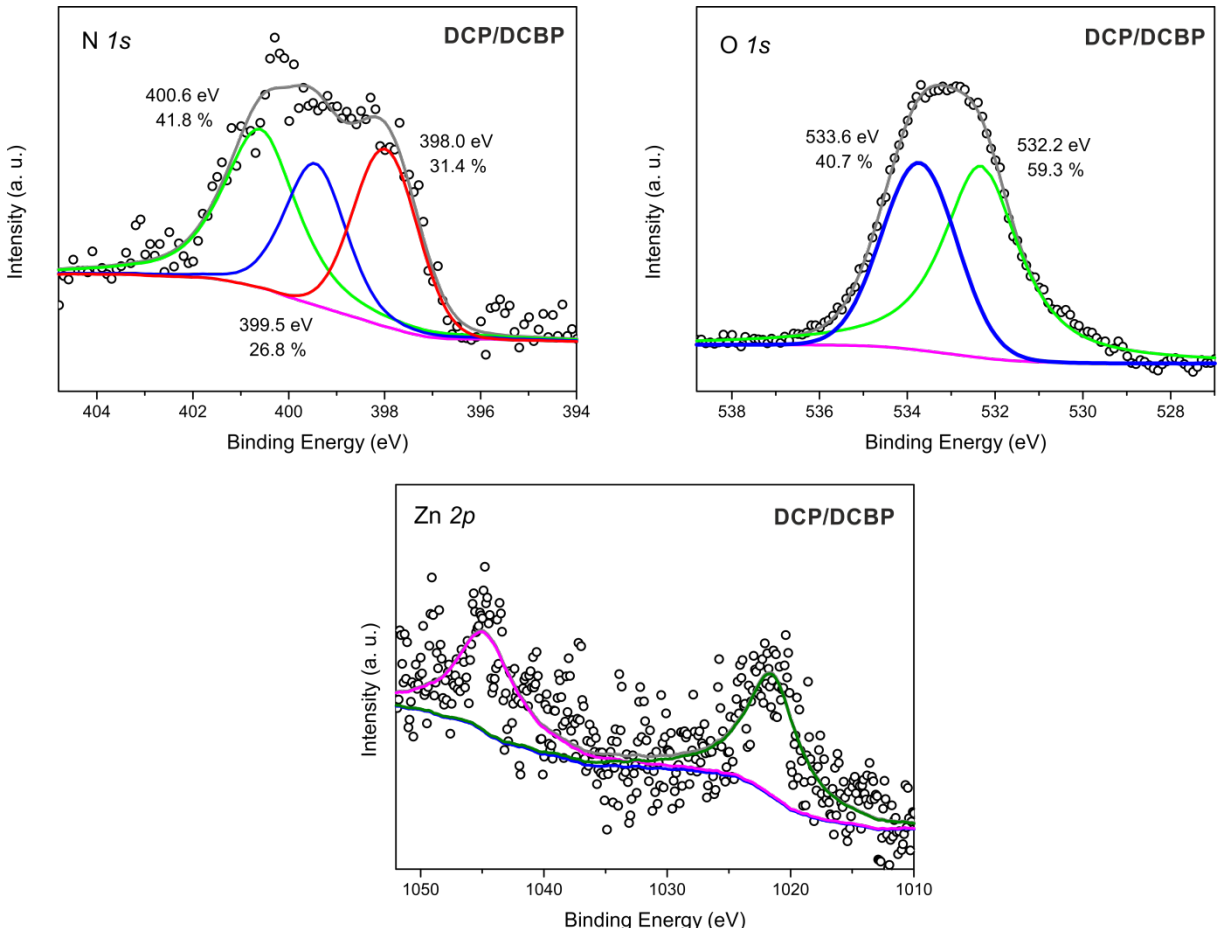

Figure S24. High resolution N1s, O1s and Zn2p core level region of DCP/DCBP sample along with their relative fitting.

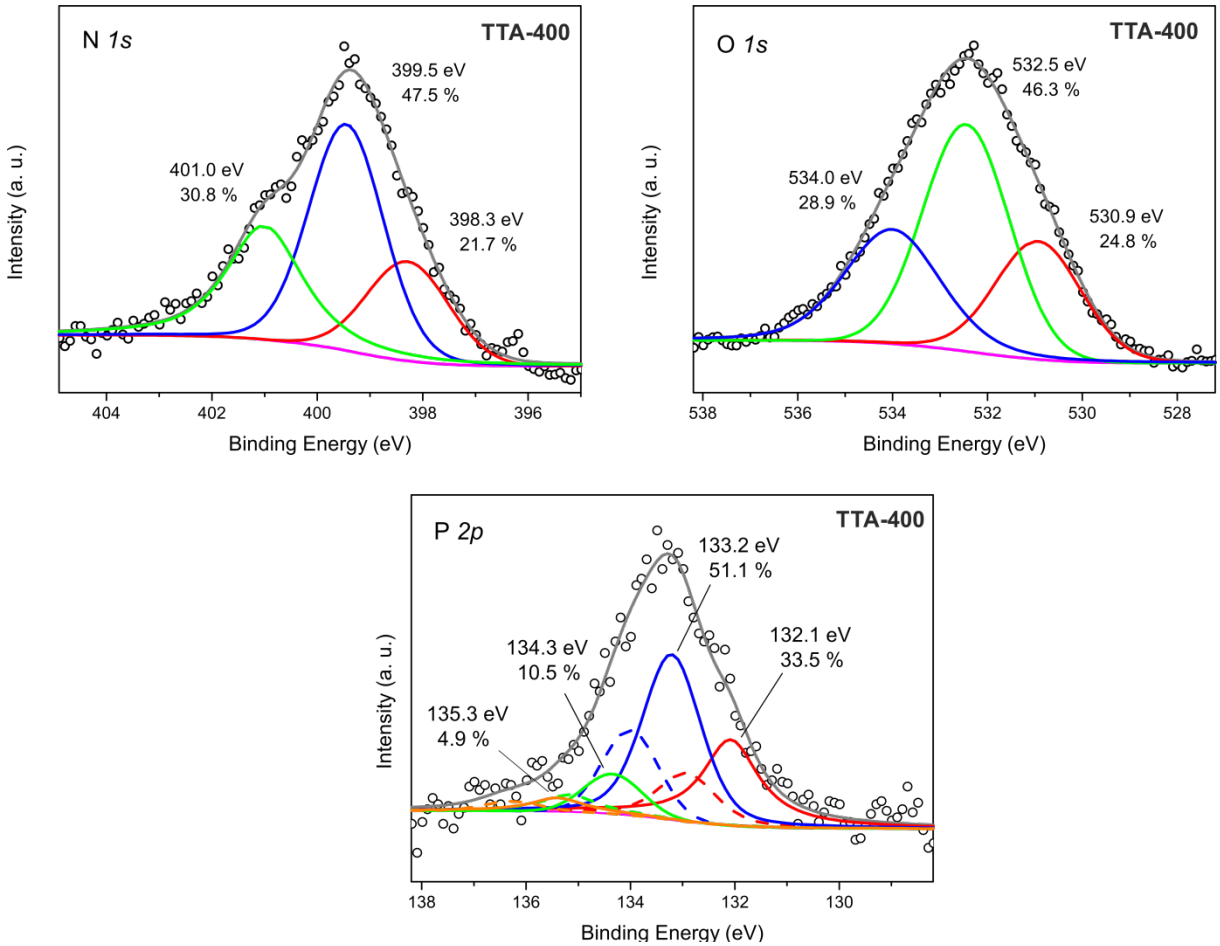

Figure S25. High resolution N1s, O1s and P2p core level region of TTA-400 sample along with their relative fitting.

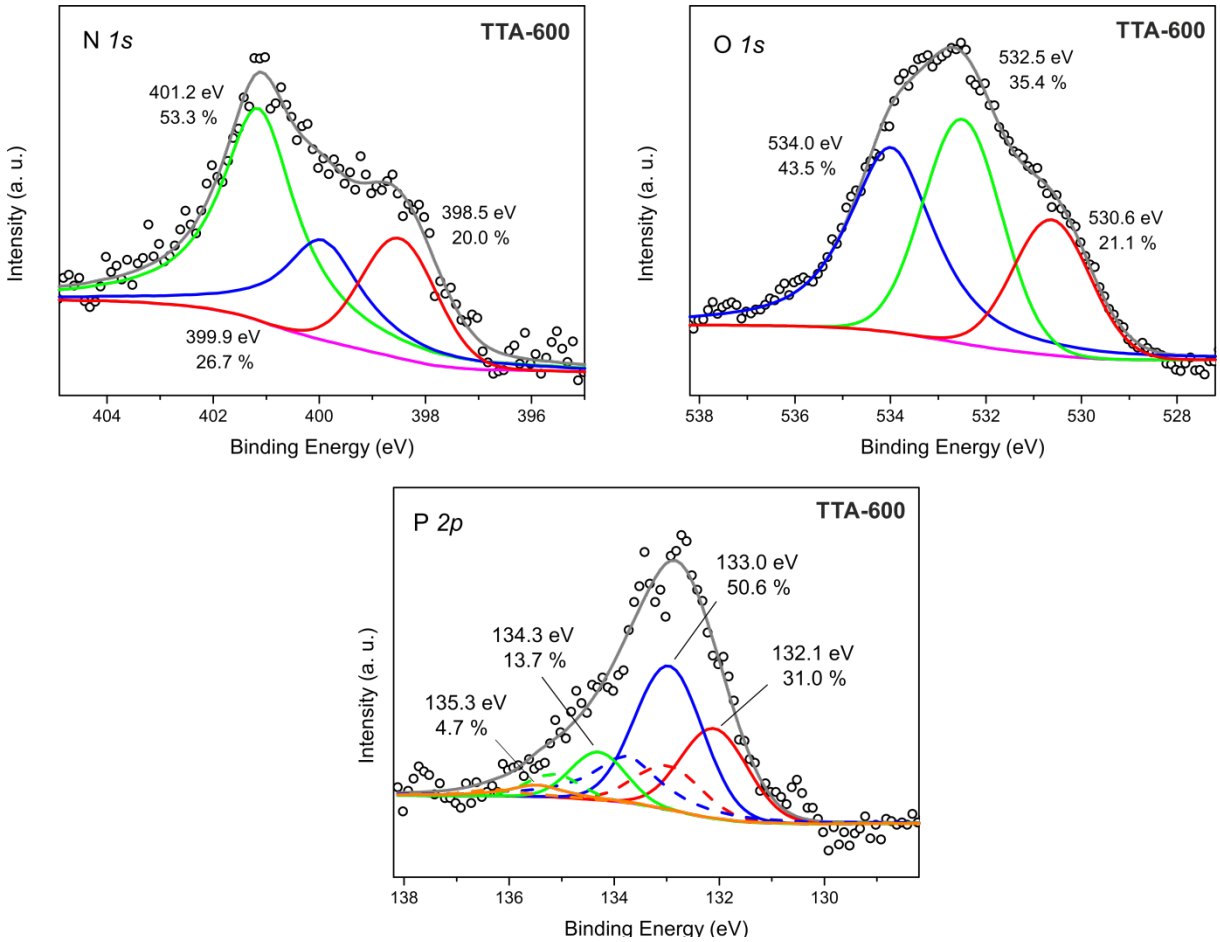

Figure S26. High resolution N1s, O1s and P2p core level region of TTA-600 sample along with their relative fitting.

Table S5. Assignment of nitrogen species during convolution of the N1s XPS signal according to Osadchii et al.[3]

Binding Energy [eV]	Assignment
398	Pyridinic Nitrogen
399-400	Pyrrolic Nitrogen
401	Graphitic Nitrogen

Table S6. Distribution of nitrogen species as determined by XPS analysis in TTA-based materials, including pDCB-600 as a comparison.

Sample	Pyridinic N [%]	Pyrrolic N [%]	Graphitic N [%]
TTA-400°C	21.7	47.5	30.8
TTA-600°C	20.0	26.7	53.3
*p*DCB-600	48.1	26.6	25.3

Table S7. Assignment of phosphorous species during convolution of the P2p XPS signal according to the work by the group of Cordéro and Wang et al.[4-6]

Binding Energy [eV]	Assignment / Linkage type
132	Phosphonate, C_3-P=O
133	Phosphonate, C_2-P-O_2, C-P-O_3
134	Phosphate, $(C\text{-}O)_x$-P-$O_{4\text{-}x}$ *(x = 1,2,3)*
135	P_4O_{10}

Table S8. Assignment of phosphorous species in ^{31}P MAS NMR spectra according to Hulicova-Jurcakova et al.[7]

Binding Energy [eV]	Assignment
-30 – -15	Polyphosphates, C-O_3-P-O
-15 – -5	Metaphosphates, C-O_2-P-O_2
~ 0	Isolated, tetra-valent phosphorous (PO_4^-)
0 – 10	Pyrophosphates, C-O-P-O_3
0 – 30	Phosphonates, C_x-P-$O_{4\text{-}x}$ *(x = 1,2,3)*

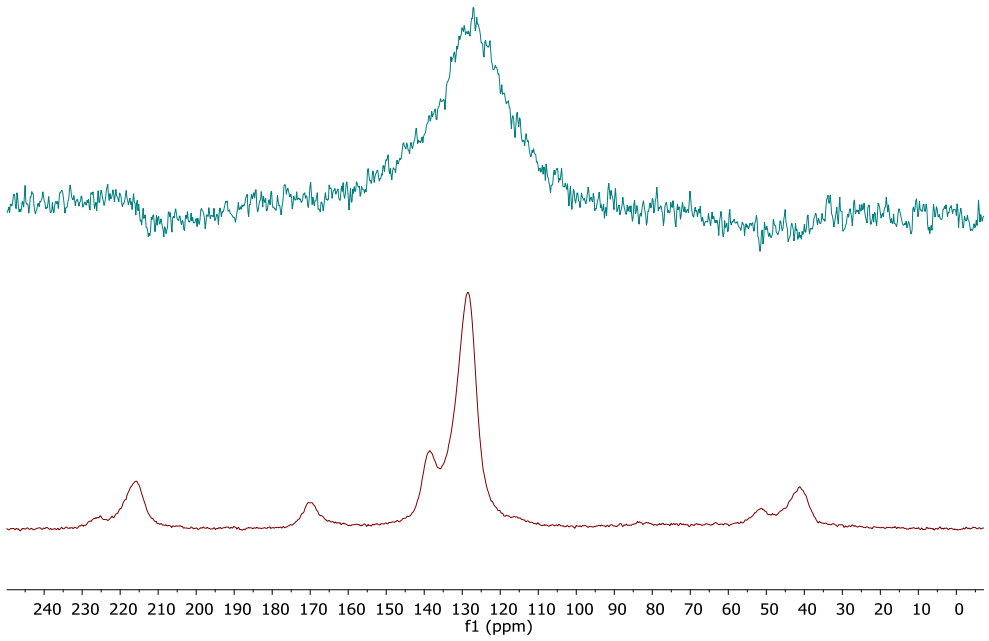

Figure S27. ^{13}C MAS NMR spectra of TTA-400 (bottom) and TTA-600 (top).

Table S9. Langmuir and Freundlich isotherm model constants and correlation coefficients for itaconic acid and glucose in multicomponent solution for CTF materials based on the $ZnCl_2$-route.

		DCP - IA	DCP - Glu	DCBP - IA	DCBP - Glu
Langmuir	R^2	0,979	0,686	0,966	0,383
	$Q\ [mg\ g_{ads}^{-1}]$	490,7	20,7	365,8	15,4
	$K_L\ [L\ mg^{-1}]$	0,05	0,58	0,60	1,05
Freundlich	R^2	0,956	0,498	0,993	0,239
	$K_F\ [g\ g_{ads}^{-1}]$	28,86	8,72	140,23	8,46
	n [ ]	1,38	3,95	3,12	5,68

Table S10. Langmuir and Freundlich isotherm model constants and correlation coefficients for lysine and glucose in multicomponent solution for CTF materials based on the $ZnCl_2$-route.

		DCP - Lys	DCP - Glu	DCBP - Lys	DCBP - Glu
Langmuir	R^2	0,984	0,829	0,951	0,874
	$Q\ [mg\ g_{ads}^{-1}]$	162,0	23,7	71,2	51,7
	$K_L\ [L\ mg^{-1}]$	0,40	3,92	0,45	1,00
Freundlich	R^2	0,994	0,850	0,977	0,899
	$K_F\ [g\ g_{ads}^{-1}]$	46,06	16,74	22,87	24,87
	n [ ]	1,90	5,80	2,19	3,11

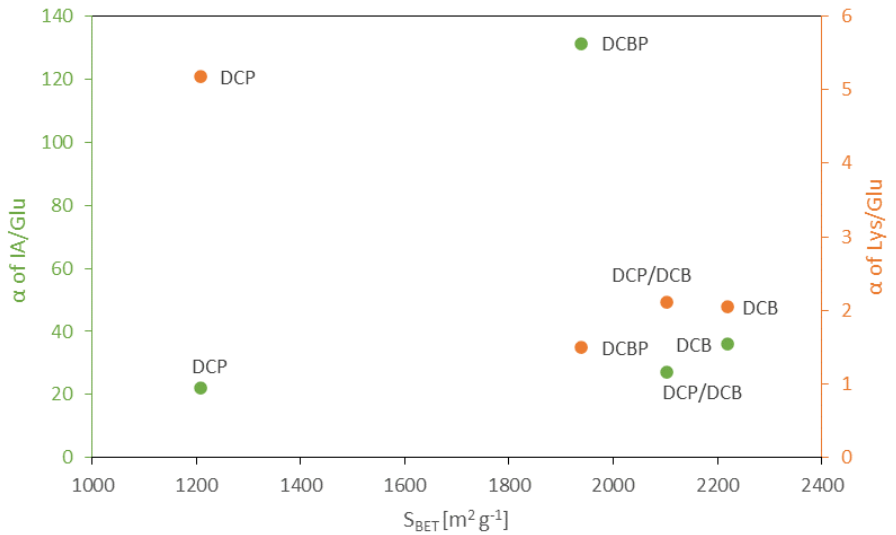

Figure S28. Correlation between the separation factor α and specific surface area of the CTFs.

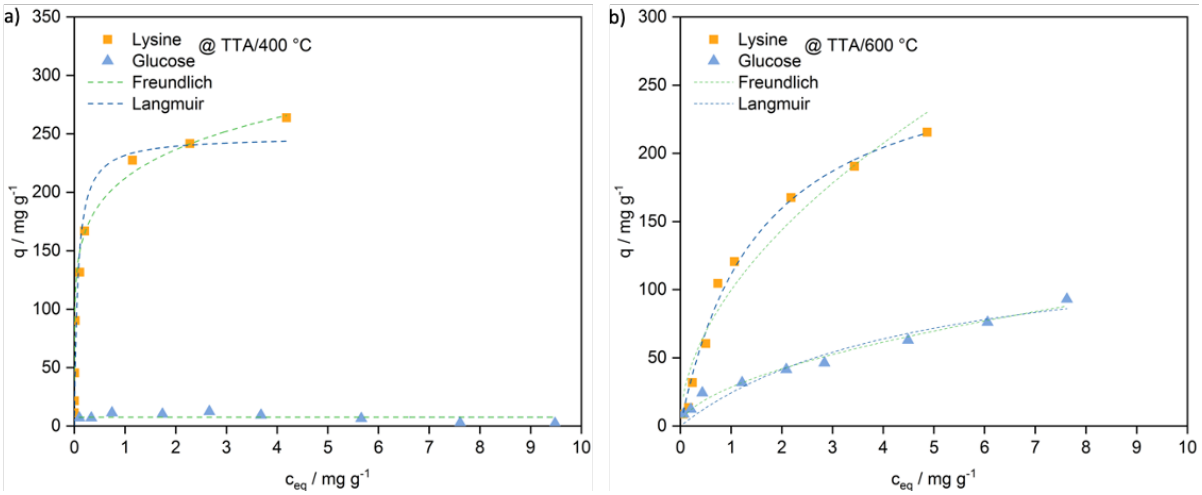

Figure S29. Competitive Adsorption Isotherms of lysine and glucose from aq. solution on TTA/400°C (a) and TTA/600°C (b) at 30 °C.

Table S11. Langmuir and Freundlich isotherm model constants and correlation coefficients for lysine and glucose in multicomponent solution for CTF materials based on the P_4O_{10}-route.

		TTA/400°C - Lys	TTA/400°C - Glu	TTA/600°C - Lys	TTA/600°C - Glu
Langmuir	**R^2**	0,964	0,003	0,989	0,943
	Q [mg g_{ads}^{-1}]	247,7	7,6	283,4	140,0
	K_L [L mg^{-1}]	14,41	446,12	0,65	0,21
Freundlich	**R^2**	0,945	0,805	0,953	-
	K_F [g g_{ads}^{-1}]	212,02	32,91	99,62	7,62
	n [ ]	6,34	5,41	1,89	-

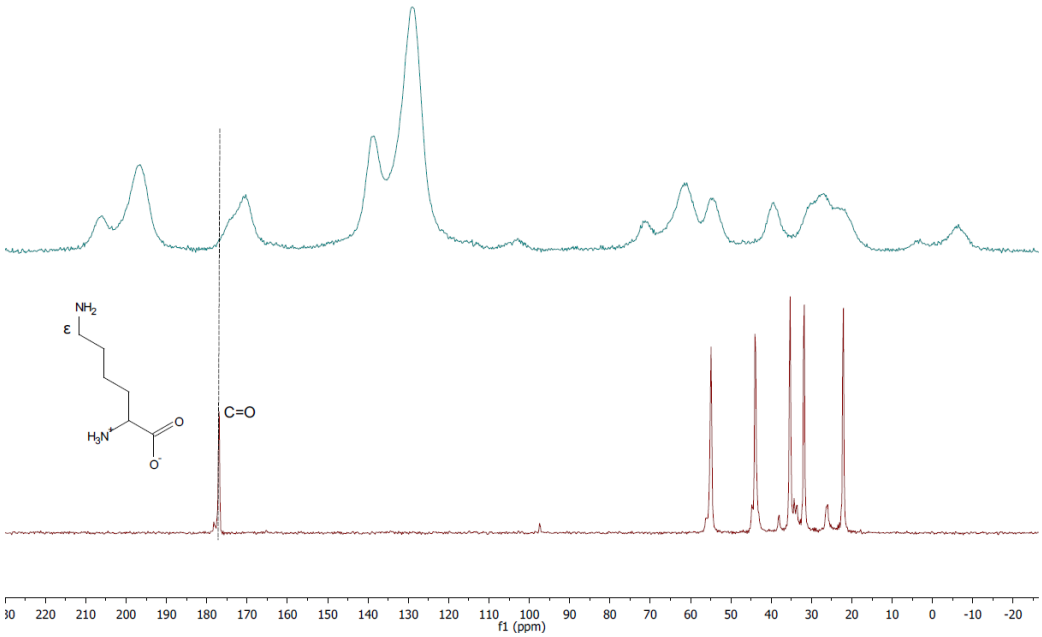

Figure S30. ^{13}C MAS NMR spectra of Lysine-TTA-400 (top) and Lysine (button) and the corresponding signal assignment.

Recycling Study

The recycling studies were conducted in a fixed-bed column setup filled with the 0.2 g CTF DCBP for IA and TTA-400 for lysine adsorption, respectively. The adsorptive aqueous solution of either lysine or IA was pumped through the fixed-bed by an HPLC pump and a feed flow rate on 1 mL min^{-1}. For desorption studies H_2O was used with a similar flow rate.

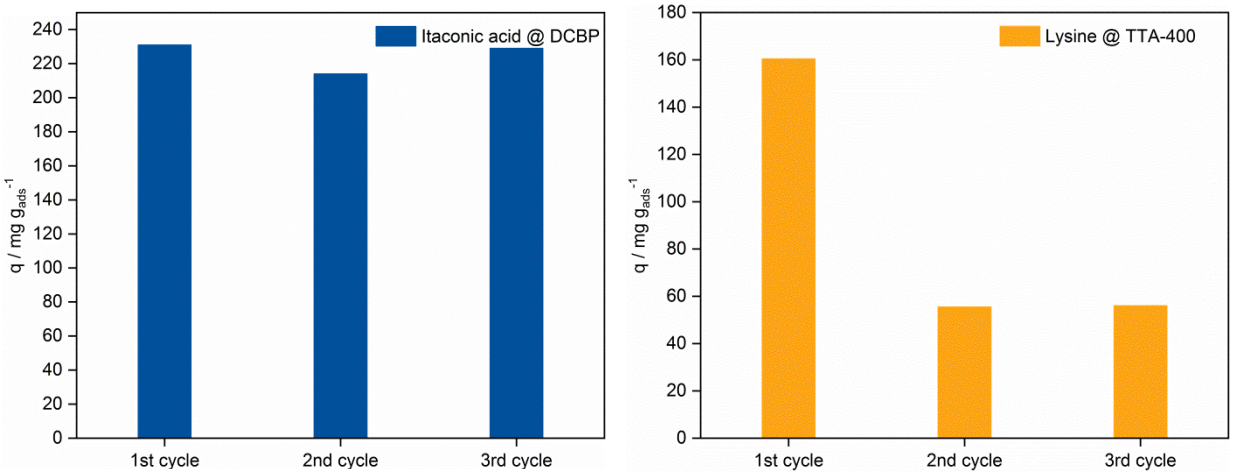

Figure S31. Adsorbed amounts of IA using DCBP (left) and adsorbed amounts of lysine using TTA-400 (right) for three consecutive adsorption cycles. $c_{Lys/IA}$ = 3 g L^{-1}.

References

1. M. S. Shafeeyan, W. M. A. W. Daud, A. Houshmand and A. Shamiri, *J. Anal. Appl. Pyrolysis*, 2010, **89**, 143-151.
2. J. L. Figueiredo, M. F. R. Pereira, M. M. A. Freitas and J. J. M. Órfão, *Carbon*, 1999, **37**, 1379-1389.
3. D. Y. Osadchii, A. I. Olivos-Suarez, A. V. Bavykina and J. Gascon, *Langmuir*, 2017, **33**, 14278-14285.
4. J. M. Rosas, R. Ruiz-Rosas, J. Rodríguez-Mirasol and T. Cordero, *Carbon*, 2012, **50**, 1523-1537.
5. A. M. Puziy, O. I. Poddubnaya, R. P. Socha, J. Gurgul and M. Wisniewski, *Carbon*, 2008, **46**, 2113-2123.
6. Y. Wang and P. M. A. Sherwood, *Surf. Sci. Spectra*, 2002, **9**, 159-165.
7. D. Hulicova-Jurcakova, M. Seredych, G. Q. Lu, N. K. A. C. Kodiweera, P. E. Stallworth, S. Greenbaum and T. J. Bandosz, *Carbon*, 2009, **47**, 1576-1584.